

Full Paper

Electrochemical Behavior Assessment of Pure Tantalum in Ringer's Physiological Solution

Arash Fattah-alhosseini* and Sareh Sharifi

Department of Materials Engineering, Bu-Ali Sina University, Hamedan 65178-38695, Iran

*Corresponding Author, Tel.: +988138292505; Fax: +98 813 8257400

E-Mail: a.fattah@basu.ac.ir

Received: 4 July 2017 / Received in revised form: 16 August 2017 /

Accepted: 13 September 2017 / Published online: 15 November 2017

Abstract- In order to evaluate the electrochemical properties of the passive film on pure Tantalum, various electrochemical methods including polarization, impedance spectroscopy and Mott–Schottky were applied in Ringer solution at 37 °C. Obtained results arisen from polarization and impedance spectroscopy measurements revealed that as the anodic passive potential increases, pure Tantalum samples passive response in Ringer solution was improved. Mott–Schottky measurements showed that the passive oxide films behaved as n-type semiconductors and passive potential cannot change the conductivity type of the passive oxide films. Moreover, Mott–Schottky measurements depicted that less donor densities in the passive film increased corrosion resistance of pure Tantalum in the test solution owing to higher anodic passive potential.

Keywords- Tantalum, Ringer solution, Polarization, Impedance spectroscopy, Mott–Schottky

1. INTRODUCTION

Among most of metals including niobium (Nb), molybdenum (Mo), tungsten (W), and rhenium (Re), except for two of the platinum (Pt)-group metals (osmium (Os) and iridium (Ir)), tantalum (Ta) is one of the refractory metals. The highest melting temperatures (>2000 °C) and the lowest vapor pressures are known as all of the refractory metals traits. Being utilized to alloying in stainless steels, cobalt (Co) alloys, and titanium (Ti) alloys is the

restricted use of nickel (Ni), Mo, W for biomedical applications. Radioactive rhenium is occasionally used in stents to prevent re-stenosis. Due to its excellent biocompatibility, flexibility and corrosion resistance, Ta has revealed a number of clinical applications [1,2].

In a large number of acids, most aqueous solutions of salts, organic chemicals and in various combinations and mixtures of these agents are known wherever Pure Ta has excellent resistance to corrosion. Ta has approximately the same corrosion resistance as glass. Ta has no known biological role, and is non-toxic. Compounds containing Ta are rarely encountered in the natural environment. Ta is among the most biocompatible metals used for implantable devices [2,3]. There is however some evidence linking Ta to local sarcomas and toxicity of its oxide to alveolar cells [4,5].

Since the 1950s, Ta has been used in surgery as suture wires for skin closure, tendon, and nerve repair [6–8]; foils and sheets for nerve anastomoses [9]; clips for the ligation of vessels [10]; staples for abdominal surgery [11,12]; and as pliable sheets and plates for cranioplasty and reconstructive surgery [13,14]. Moreover, sintered Ta capacitor electrodes are used in electrical stimulation devices [15]. Ta has been used to coat other metals, such as Ti implants [16], and carbon (C) foam skeletons used also as a biocompatible replacement for vertebral bodies of the spinal column [17]. Ta coatings, which are 70–80% porous, have a macroporous structure similar to that of cancellous bone [16–18]. Besides, spinal implants, carbon–tantalum (C-Ta) cellular materials have potential applications for hip and knee construction and bone scaffold void filling applications. Also, porous scaffolds have been made from Ta, including Trabecular metal, which contains pores, the size of which makes this material very good for bone in-growth. It is believed that Trabecular Metal has an elastic nature which aids bone remodeling [19–21].

Considering the investigations have been done on the corrosion behavior of Ta, it is found that the electrochemical behavior of this metal in Ringer solution is less studied. Thus, the main purpose of this study is to evaluate the passive behavior of Ta in Ringer solution from electrochemical viewpoint by potentiodynamic polarization (PDP), electrochemical impedance spectroscopy (EIS) and Mott–Schottky (M–S) analysis.

2. EXPERIMENTAL PROCEDURES

Before any electrochemical measurements, pure Tantalum specimens were ground to 1800 grit and double cleaned by distilled water. The exact details of flat cell and all electrochemical (PDP, EIS and M–S) measurements were published elsewhere [22,23]. To investigate the electrochemical properties of the passive film on pure Tantalum in Ringer solution at 37 °C, we chose four potentials (0.1, 0.3, 0.5 and 0.7 V_{Ag/AgCl}) within the passive region. Time duration for oxide film growth was considered 900 s to make sure that the steady-state condition is on. All electrochemical tests were repeated at least three times.

Moreover, to provide the EIS data with the appropriate fitted curves, NOVA 2.0.2 impedance software was used.

3. RESULTS AND DISCUSSION

3.1. Open-circuit potential (OCP) and polarization measurements

OCP vs. time plot of pure Tantalum sample in the test solution is shown in Fig. 1. As seen, at the start of immersion, the OCP is directed towards positive values. This trend is reported for pure Tantalum in 0.1 M H₂SO₄ solution, which indicates the formation of passive oxide film and its role in increasing protectivity with time [23]. The OCP curves show that within 2400 s a complete stable condition is achieved to implement the electrochemical tests. PDP curve of pure Tantalum sample in the test solution is showed in Fig. 2.

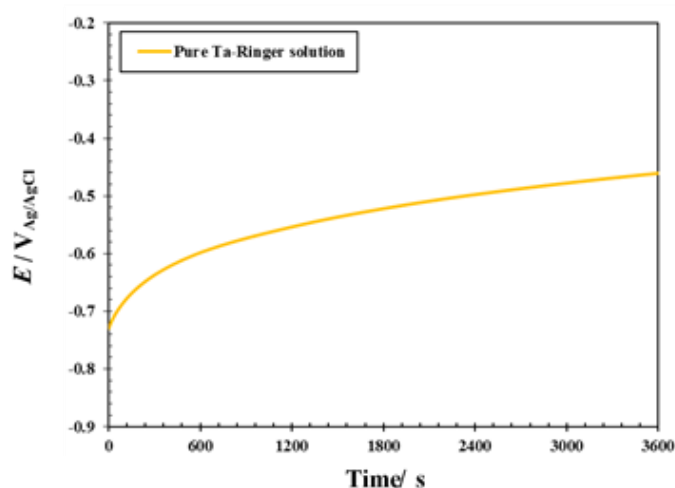


Fig. 1. OCP curve of pure Tantalum in Ringer's physiological solution at 37 °C

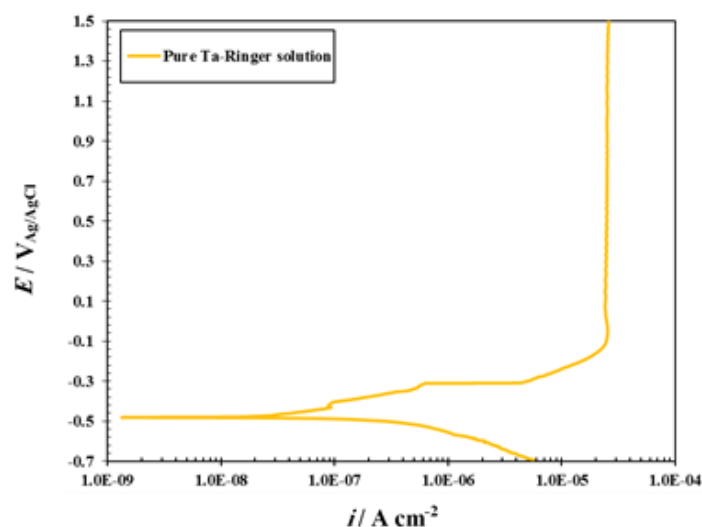


Fig. 2. PDP plot of pure Tantalum in Ringer's physiological solution at 37 °C

Clearly, pure Tantalum sample is spontaneously passivated in Ringer solution. Similar PDP curve is observed for this metal in acidic and basic solutions [22-24]. Fig. 3 reveals the potentiostatic polarization and steady-state passive current density (i_{ss}) plots for pure Tantalum sample. As seen, the current density weakens with time until a steady-state is established. Fig. 3(b) shows the rates of the steady-state passive current density versus the anodic passive potential. The mean steady-state current density is $0.711 \times 10^{-6} \text{ A cm}^{-2}$.

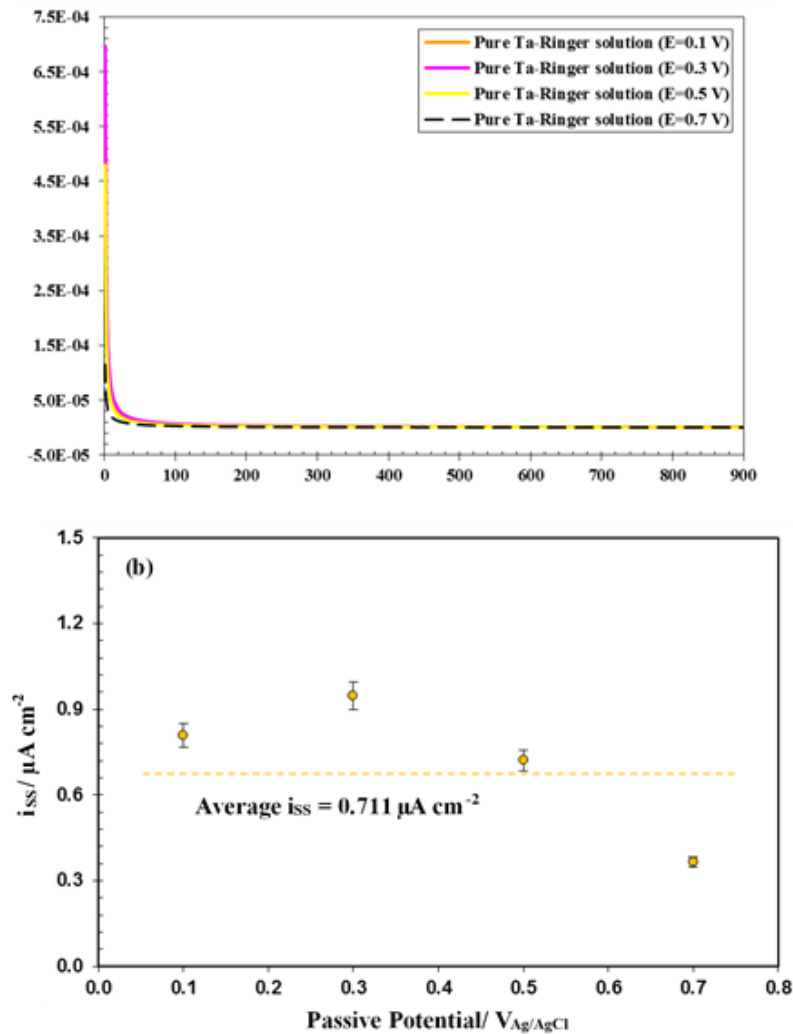


Fig. 3. (a) Potentiostatic polarization and (b) steady-state passive current density plots of pure Tantalum in Ringer's physiological solution at 37 °C

3.2. M–S analysis

Effect of passive potential on the passive films formed on pure Tantalum specimens was determined and M–S curves (Fig. 4) were obtained to determine the donor density (N_D) by using Eq. (1) [22,23]:

$$\frac{1}{C^2} = \frac{2}{\epsilon \epsilon_0 e N_D} \left(E - E_{fb} - \frac{k_B T}{e} \right) \tag{1}$$

In this equation, ϵ is the dielectric constant of passive layer (25 for Ta [22-25]), ϵ_0 shows the vacuum permittivity, e is the electron charge, k , T , and E_{fb} show the Boltzmann constant, absolute temperature, and flat band potential, respectively. By extrapolating linear portion to $C_{sc}^{-2}=0$, one can determine the flat band potential. It is interesting to note that E_{fb} decreases as the anodic passive potential increase. Obviously, it is observed that as the anodic passive potential increase, the capacitance of pure Tantalum samples decreases. Similar M–S plots are observed for this metal in acidic and basic solutions [22-24].

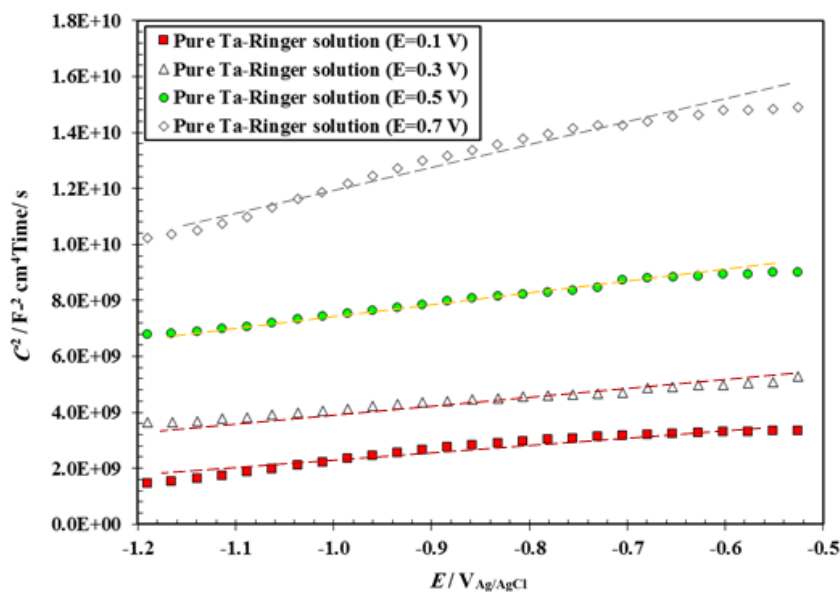


Fig. 4. M–S plots of pure Tantalum in Ringer’s physiological solution at 37 °C

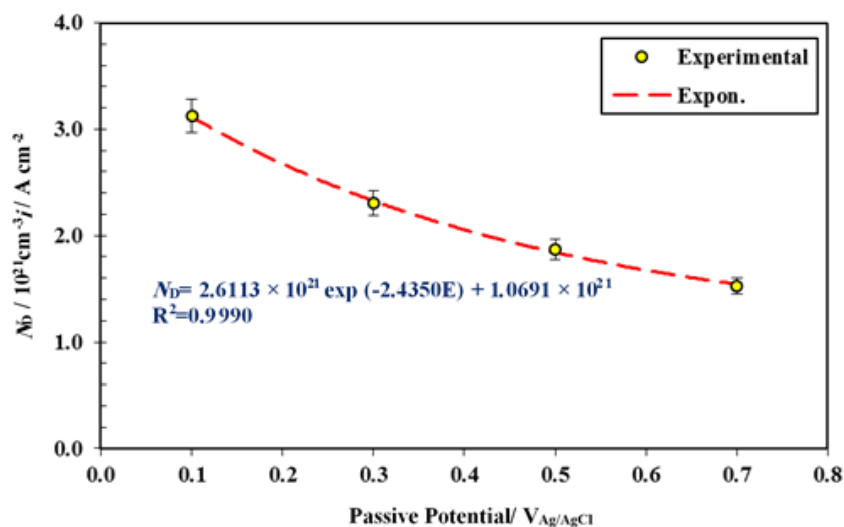


Fig. 5. Calculated donor density of the passive films formed on pure Tantalum in Ringer solution

Fig. 5 shows the effect of anodic passive potential on the calculated donor densities of pure Tantalum samples. Obviously, the values of donor densities are in the order of 10^{21} cm^{-3} , this is analogous with the reports in literature [22-24]. It must be mentioned that the exact value of donor densities depends on the thickness of the passive film and the applied solution as an electrolyte [22-24].

The PDM showed that the defect structure of the passive layer can be ascribed by a series of defect generation and annihilation reactions happening at the interface of metal and the passive layer and at the interface of the passive layer and the solution [26]. The values gained through M-S analysis depicted that the calculated values of donor densities decrease by passive potential (Fig. 5). In addition, the electrochemical reactions are dependent to electron transmission, and decrease in donor density can limit the electron transfer, the result can be depicted as marked inhibition of electrochemical reactions. Thus, passive layer dissolution slows down and fewer defects and preferable protective capacity are obtained [22-24]. Indeed, lower defects in passive layer, less mass transport and better corrosion resistance will become clear. Also, it is revealed by Fig. 5 that while anodic passive potential increases, the donor density of pure Tantalum samples reduces. Moreover, considering other literature shows that decrease in donor density occurs while the anodic passive potential increases. Here, it must be said that the potential-independent current (i_{ss}) and the potential-dependent N_D together because donor density at the metal/passive layer interface has significant impact on the current density [22-24].

Noting the PDM, existence of non-stoichiometry defects within the passive films, changes defect density. Fig. 4 depicts pure Tantalum samples n-type behavior in in Ringer solution. Thus, it can be explained that oxygen vacancies and/or the cation interstitials donate electrons and as a result negative conduction type in passive layer is created [13,14]. In the formed passive layers, higher density of the oxygen vacancies and/or the cation interstitials is the major reason for the increased donor density values. Eq. (2) reveals the relation between donor density and anodic passive potential [26-29]:

$$N_D = \omega_1 \exp(bE) + \omega_2 \quad (2)$$

Here, ω_1 , ω_2 and b are unknown constants specified according to the experimental records.

3.3. EIS measurements

Fig. 6 depicts the role of anodic passive potential on the EIS plots of pure Tantalum samples in the test solution. For all passive potential, just one capacitive loop is seen (Fig. 6(a)). As seen, all Nyquist plots show imperfect semicircles. Also, the Bode plots (Fig. 6(b)) shows a marked capacitive response (in the middle to low frequency range) and a resistive behavior (at high frequency range). In addition, in the intermediate frequency region, the Bode-phase plots (Fig. 6(c)) reveals the constant phase behavior. The values of phase angle

(Fig. 6(c)) remained close to 90 and showed the formation and growth of the passive layer [22-24]. All plots depict the augmentation of phase angle in the intermediate frequency region as the passive potential increased.

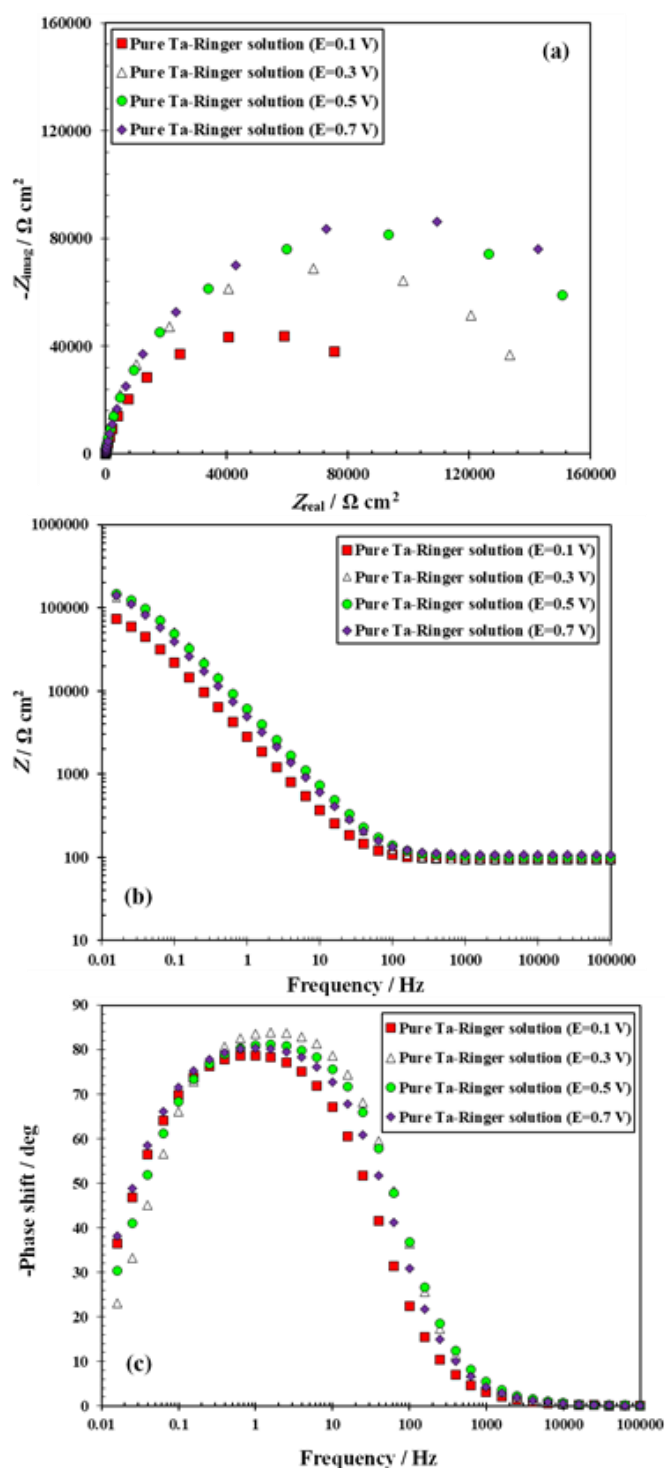


Fig. 6. Role of passive potential on the (a) Nyquist; (b) Bode plots, and (c) Bode-phase plots

This evolution depicted the formation and growth of passive layers [22-24]. Moreover, with passive potential, impedance in the low frequency region increased. Fig. 7 shows a comparison between the EIS data and those obtained from Kramers–Kronig (K–K) transformation. The exact details of K–K transformation were published elsewhere [22-24]. As seen, the latter is well in tandem with the former that confirms that the system acts in accordance with the prerequisites of linear system theory.

For fitting the impedance spectra, the equivalent electrical circuit (EEC) showed in Fig. 8 was applied. In this EEC, R_s is the solution resistance, R_p reveals the resistance of the oxide passive layer, and Q_p is constant phase element (CPE) relating to the capacitance of the passive layer [22-24]. The impedance and the capacitance of the CPE are obtained through the following equation [30]:

$$Z_{CPE} = [Q(j\omega)^n]^{-1} \quad (3)$$

$$C = Y_0(\omega_{max})^{n-1} \quad (4)$$

The exact details of Eq. (3) and (4) were published elsewhere [22-24].

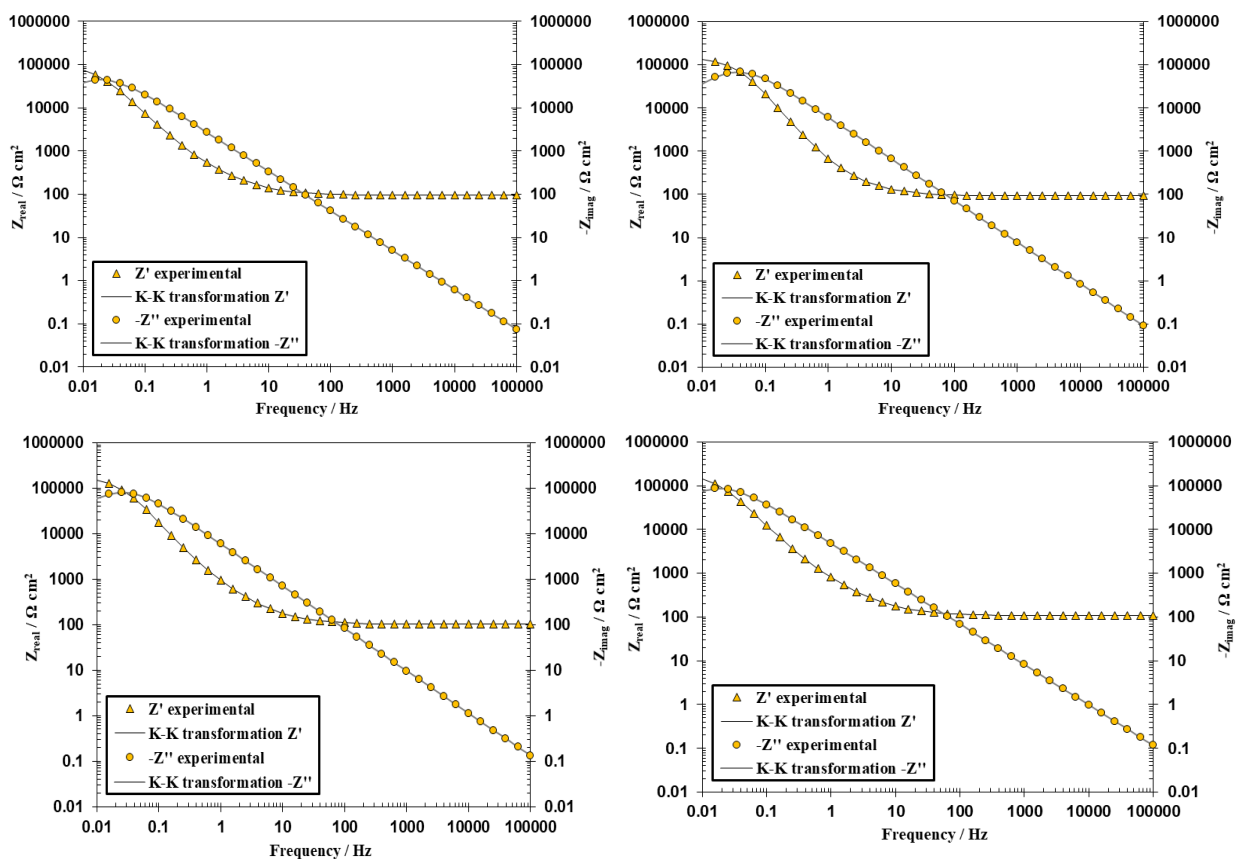


Fig. 7. Role of passive potential on the K–K transformation of the EIS data: (a) 0.1, (b) 0.3, (c) 0.5, and (d) 0.7 V_{Ag/AgCl}

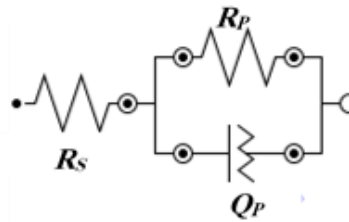


Fig. 8. Equivalent electrical circuit used to model the experimental EIS data

Fig. 9 depicts the effect of passive potential on the resistance and capacitance of the passive layers of pure Tantalum in Ringer solution. As seen, the resistance of the passive layer increases by passive potential (Fig. 9 (a)). Moreover, noting the Fig. 9(b), it is observed that by increasing the passive potential, the passive film capacitance decreases. Generally, drop in the passive film capacitance depicts lower dissolution and the passivity increase [22-24].

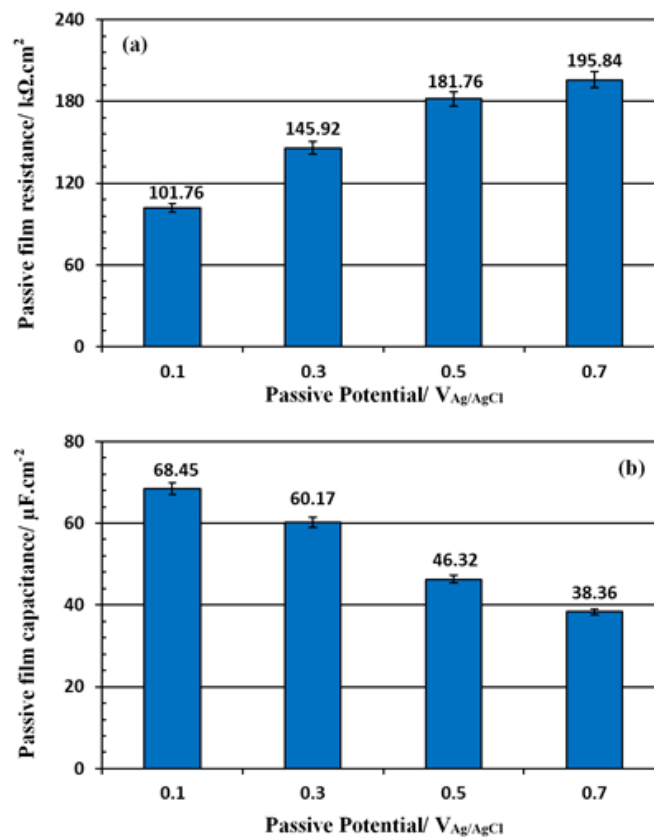


Fig. 9. Role of passive potential on the (a) passive film resistance and (b) passive film capacitance of pure Tantalum in the test solution.

Eq. (5) is used to calculate the thickness of the passive layer (L) [22-24,31]:

$$L = \frac{\varepsilon_0 A}{C} \quad (5)$$

The exact detail of Eq. (7) was found elsewhere [22-24]. Fig. 10 reveals the effect of passive potential on the passive layer thickness of pure Tantalum in the test solution. Clearly, it is seen that as the passive potential increase, the passive film thickness increases. The calculated passive layer thickness is in the range of 0.8-1.8 nm, which is agreement with those reported in the literature for pure Tantalum in other solutions [22-24]. Generally, the linear potential-dependent relation of passive layer thickness is found experimentally on pure Tantalum in other solutions [22-24]. The anodic passive potential and passive film thickness in the point defect model (PDM) have the following relationship in Eq. (6) [22-24]:

$$L = \frac{1-\alpha}{\varepsilon_L} E + \beta \quad (6)$$

Here, β depicts a depending upon the pH, α is the polarizability of the passive layer/solution interface, and ε_L shows the passive film electric field strength. The electric field is identified to be independent of the anodic passive potential and passive layer thickness [22-24]. The gradient for pure Tantalum sample obtained from Fig. 10 was 1.245 nm/V. Thus, the calculated electric field strength of pure Tantalum sample is 0.401×10^6 V/cm.

Through fitting of the experimental findings, the exponential relationship between N_D and E is obtained as Eq. (7) [26,27]:

$$N_D = 2.6113 \times 10^{21} \exp(-2.4350E_{ff}) + 1.0691 \times 10^{21} (\text{cm}^{-3}) \quad (7)$$

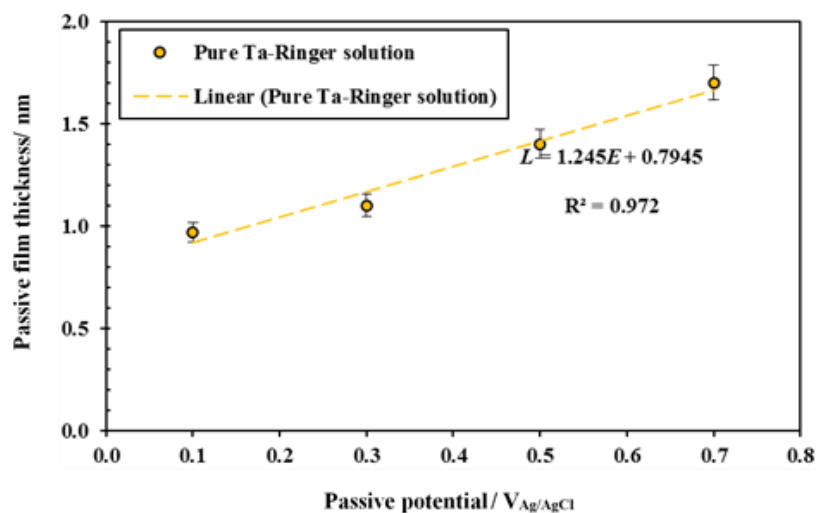


Fig. 10. Role of passive potential on the passive film thickness of pure Tantalum in the test solution

Eq. (8) expresses the calculation of the diffusion [26,27]:

$$D_0 = -\frac{i_{ss}RT}{4eF\omega_2\varepsilon_L} \quad (8)$$

Here, R and F show the ideal gas constant and the Faraday constant. By substituting i_{ss} , ε_L , and ω_2 into Eq. (8), one can find $D_0 = 0.665 \pm 0.05 \times 10^{-18}$. Thus, the diffusion coefficient of defects in the passive film formed on pure Tantalum in the test solution is estimated in the range of 10^{-18} cm²/s. This is in the order of the results recorded for defects diffusion coefficient in the passive film for pure Tantalum in acidic and basic solutions [22-24].

4. CONCLUSION

Conclusions of the current investigation are as below:

1. Potentiostatic polarization plots showed that the steady-state current density was independent of the film formation potential that is in complete accordance with the PDM postulation.
2. M-S analysis was carried out in order to determine the passive films semiconducting behavior. Revealed results showed while formation potential grows, donor density values exponentially decline and the passive films thickness linearly increases.
3. Produced results by M-S analysis showed that the experimental data were justified in terms of the PDM for the passivity of pure Tantalum in Ringer solution. The calculated diffusivity of defect was in the range of 10^{-18} cm²/s.

REFERENCES

- [1] U. O. Hafeli, M. C. Warburton, and U. Landau, *Biomaterials* 19 (1998) 925.
- [2] Q. Chen, and G. A. Thouas, *Mater. Sci. Eng. R* 87 (2015) 1.
- [3] J. Black, *Clin. Mater.* 16 (1994) 167.
- [4] B. S. Oppenheimer, E. T. Oppenheimer, I. Danishefsky, and A. P. Stout, *Cancer Res.* 16 (1956) 439.
- [5] R. A. Matthay, P. A. Balzer, C. E. Putman, J. B. Gee, G. J. Beck, and R. H. Greenspan, *Invest. Radiol.* 13 (1978) 514.
- [6] S. Brumme, G. Lowicke, and W. Knofler, *Z. Exp. Chir. Transplant. Kunstliche Organe* 22 (1989) 308.
- [7] M. Khalid, *Minerva Urologica e Nefrologica* 17 (1981) 49.
- [8] T. V. Kalinina, and O. R. Bogomolova, *Voprosy Neurokhirurgii* 23 (1959) 41.
- [9] S. Bando, *Kobe Ika Daigaku Kiyo* 26 (1964) 98.
- [10] T. V. Kalinina, *Khirurgiia* 44 (1968) 97.
- [11] M. F. Vyrzhikovskaia, *Eksp Khir* 4 (1959) 38.
- [12] M. G. Anan'Ev, N. V. Antoshina, and I. I. Gritsman, *Eksp. Khir* 2 (1957) 28.
- [13] A. H. Andrews Jr., and M. J. Tamari, III *Med. J.* 103 (1953) 175.

- [14] R. Molicki, B. Klapotocz, M. Sypniewski, and E. Wierzynski, *Czas. Stomatol.* 32 (1979) 595.
- [15] I. Arcos, R. Davis, K. Fey, D. Mishler, D. Sanderson, C. Tanacs, M.J. Vogel, R. Wolf, and Y. Zilberman, *J. Schulman, Artif. Organs* 26 (2002) 228.
- [16] V. K. Balla, S. Banerjee, S. Bose, and A. Bandyopadhyay, *Acta Biomater.* 6 (2010) 2329
- [17] S. Eriksen, B. Gillesberg, L. N. Langmaack, E. Christensen, H. Li, M. Lind, C. Bunger, Tantalum coated carbon-carbon composite material for surgical implants, in: *Medical Device Materials II: Proceedings of the Materials & Processes for Medical Devices Conference 2004*, ASM International, MaterialsPark, OH, (2005) pp. 245–250.
- [18] S. Dittrick, V. K. Balla, S. Bose, and A. Bandyopadhyay, *Mater. Sci. Eng. C* 31 (2011) 1832.
- [19] P. S. Nebosky, and S. R. Schmid, *J. Manuf. Sci. Eng. Trans. ASME* 133 (2011).
- [20] D. A. J. Wilson, G. Richardson, A. W. Hennigar, and M. J. Dunbar, *Acta Orthop.* 83 (2012) 36.
- [21] A. Sternheim, D. Backstein, P. R. T. Kuzyk, G. Goshua, Y. Berkovich, O. Safir, and A. E. Gross, *J. Bone Joint Surg. Am.* 94B (2012) 158.
- [22] A. Fattah-Alhosseini, F. R. Attarzadeh, S. Vafaeian, M. Haghshenas, and M. K. Keshavarz, *Int. J. Refract. Met. Hard Mater.* 64 (2017) 168.
- [23] A. Fattah-alhosseini, S. Vafaeian, A. R. Ansari, and M. Khanmohammadi, *Anal. Bioanal. Electrochem.* Accepted manuscript 9 (2017) 660.
- [24] F. R. Attarzadeh, N. Attarzadeh, S. Vafaeian, and A. Fattah-Alhosseini, *J. Mater. Eng. Perform.* 25 (2016) 4199.
- [25] J. Xu, W. Hu, S. Xu, P. Munroe, and Z. H. Xie, *ACS Biomater. Sci. Eng.* 2 (2016) 73.
- [26] E. Sikora, J. Sikora, and D. D. Macdonald, *Electrochim. Acta* 4 (1996) 783.
- [27] A. Fattah-alhosseini, *Arab. J. Chem.* 9 (2016) S1342.
- [28] J. Liu, and D. D. Macdonald, *J. Electrochem. Soc.* 148 (2001) B425.
- [29] S. Z. Smialowska, W. Kozlowski, *Passivity of Metals and Semiconductors*, Netherlands (1983).
- [30] B. Hirschorn, M. E. Orazem, B. Tribollet, V. Vivier, I. Frateur, and M. Musiani, *Electrochim. Acta* 55 (2010) 6218.
- [31] W. Wang, F. Mohammadi, and A. Alfantazi, *Corros. Sci.* 57 (2012) 11.